

Hydrological Sciences Journal

ISSN: 0262-6667 (Print) 2150-3435 (Online) Journal homepage: www.tandfonline.com/journals/thsj20

Avulsion distribution on rivers in the Himalayan foreland region

Rajesh Kumar Sah, D. Nagesh Kumar & Apurba Kumar Das

To cite this article: Rajesh Kumar Sah, D. Nagesh Kumar & Apurba Kumar Das (2022) Avulsion distribution on rivers in the Himalayan foreland region, Hydrological Sciences Journal, 67:14, 2175-2190, DOI: 10.1080/02626667.2022.2136000

To link to this article: https://doi.org/10.1080/02626667.2022.2136000

View supplementary material

Published online: 11 Nov 2022.

Submit your article to this journal

Article views: 765

View related articles

View Crossmark data

Citing articles: 2 View citing articles

Full Terms & Conditions of access and use can be found at
https://www.tandfonline.com/action/journalInformation?journalCode=thsj20

HYDROLOGICAL SCIENCES JOURNAL
2022, VOL. 67, NO. 14, 2175–2190
https://doi.org/10.1080/02626667.2022.2136000

Check for updates

Avulsion distribution on rivers in the Himalayan foreland region

Rajesh Kumar Sah[a], D. Nagesh Kumar[a] and Apurba Kumar Das[b]

[a]Department of Civil Engineering, Indian Institute of Science, Bengaluru, India; [b]School of Sciences, Department of Environmental Science, Tezpur University, Tezpur, India

ABSTRACT

Despite recent advances, we still do not have a synoptic dataset on river avulsion across a mountain foreland belt. Here we report a novel account of chronological avulsion records (for the period 1990–2019) across the Himalayan foreland region (HFR), one of the largest and most avulsion-hit areas in the world. The chronological records discerned river avulsion frequency and distribution across HFR. We identified the eastern Brahmaputra plains as amongst the most avulsion-affected areas in HFR. As many as 19 tributaries across HFR have recorded ≥ 6 avulsion events. Most of these avulsion-affected rivers are smaller, with hilly catchments < 500 km^2. These avulsions often occurred near the proximity of the Himalayan front. Transitional reaches (and adjacent braided/meandering sections) of the tributaries have experienced higher avulsions. Observation suggests that the 1950 Assam earthquake, non-incised channels, and rapid transition in tributaries' morphologies are decisive in the region's frequency and distribution of river avulsions.

ARTICLE HISTORY
Received 25 June 2022
Accepted 9 September 2022

EDITOR
A. Fiori

ASSOCIATE EDITOR
M. Nones

KEYWORDS
Himalayan foreland river; Ganga–Brahmaputra alluvial plain; river avulsion frequency; non-incised channel; 1950 Assam earthquake

1 Introduction

The frequencies of avulsion vary among rivers (Slingerland and Smith 2004, Edmonds *et al.* 2016). Globally, observations of historical and modern river avulsion events suggest that their frequencies vary from a few to several thousand years (Wang and Liang 2000, Aslan *et al.* 2005, Tooth *et al.* 2007, Lombardo 2016, Sah and Das 2018). From these works, we can recognize that avulsions are common in the lower reaches–deltaic regions and the mountain forelands of the rivers. Besides playing a pivotal role in floodplain formation, avulsions repeatedly lead to riverine hazards affecting various stakeholders (e.g. Sinha 2009, Syvitski and Brakenridge 2013). Therefore, it is essential to understand the avulsion distribution and frequency for sustainable river management (Lombardo 2016, Sah and Das 2018, Li *et al.* 2022). However, the difficulty of obtaining data on natural river avulsion is an obstacle to developing such an understanding. This is because direct observations of natural river avulsions are rare (Valenza *et al.* 2020, Brooke *et al.* 2022). This reflects the current status of research in river avulsion distribution. Studies on the avulsion distributions of the rivers across a region are still few and require efforts from scientists across the globe.

If we look at global avulsion studies, unsurprisingly, a major chunk of the works are focused on the Himalayan foreland region (HFR). This is because of the recurring nature of avulsions in the region's rivers. The parent channels of Indus, Ganga, and Brahmaputra, the three primary river systems that flow along the Himalayan foreland, have suffered several avulsions in the last three centuries. The palaeochannels of Indus suggest numerous avulsions, including the catastrophic one in 2010 (Flam 1993, Syvitski and Brakenridge 2013). However, major avulsion in the Ganga has only been reported once, having taken place about three to four centuries in the past (Gupta *et al.* 2014). The Brahmaputra, the eastern river of the Himalayan foreland, had avulsed twice in the last three centuries (Coleman 1969, Sarma and Phukan 2004). Apart from the trunk channels of the three major river systems of the Himalayan foreland, their tributaries were also reported to be dynamic. Kosi, a major tributary of Ganga, has an avulsion frequency of 28 years (Slingerland and Smith 2004 and the reference therein). Reconstruction of the avulsions based on maps and satellite imagery reflected eight major and several minor events in 230 years in Bagmati, another tributary of Ganga (Jain and Sinha 2003). An investigation into the Sarda River system led (Mitra *et al.* 2005) to infer that it avulsed over 10 to 100 years. Manas, a major tributary of Brahmaputra, has avulsed four times in the last <300 years (Sah *et al.* 2022). A relatively detailed study on modern river avulsion across Brahmaputra plains identified three foreland rivers – Jiadhal, Gai, and Simen – having avulsion frequencies of 5 years or less (Sah and Das 2018).

The literature review suggests there have been extensive avulsion studies on the HFR but that they have mainly concentrated on isolated rivers or particular rivers from specific avulsion-prone areas. The availability of regular satellite imagery and data makes modern river avulsion studies more explicit (Sah and Das 2018). In the Himalayan foreland, such a study is more practical because of the abundance of avulsion events. Yet chronological research encompassing rivers across the Himalayan foreland region is missing. Such a dataset would allow us to identify the avulsion-active belts in the Himalayan foreland and reveal the avulsion frequency in different-sized rivers, which has rarely been explored.

CONTACT Rajesh Kumar Sah rajeshkumarxah@gmail.com Department of Civil Engineering, Indian Institute of Science, Bengaluru 560012, India
Supplemental data for this article can be accessed online at https://doi.org/10.1080/02626667.2022.2136000
© 2022 IAHS

Avulsions vary from river to river and along their longitudinal span. A preliminary examination of published works reveals that studies focusing on longitudinal avulsion distribution on rivers across a region are rare. Valenza *et al.* (2020) took 63 avulsions from three basins (Andean, Himalayan, and New Guinean) and correlated their avulsion styles with channel morphology and systematical downstream changes. However, their research was limited to a few rivers in the Himalayan foreland and did not look into the chronological records. Without knowing the chronological avulsion records, the longitudinal avulsion distribution along a river cannot be calculated correctly.

We report a chronological avulsion record from 110 HFR rivers flowing along the Ganga-Brahmaputra alluvial plain captured in Landsat imagery. The avulsion record is used to answer some critical questions: (a) Which are the avulsion-active areas in the HFR? (b) Does the avulsion frequency vary with the sizes of the rivers? (c) How were the avulsions distributed in the rivers longitudinally? We also discuss the factors playing critical roles in the river avulsion-active areas in the HFR.

2 Study area and its hydro-geomorphic settings

The study area is located between 24° and 30°15′ N latitude and between 78°20′ and 95°25′E longitude and covers a major portion of the expanse of the HFR (Fig. 1). Rainfall, one of the crucial triggers of river avulsion, is higher in the eastern Himalayan region than in the central and western regions (Fig. 2(a)). The right-bank Brahmaputra valley receives 2359 mm of annual rainfall compared to 1269 mm of annual rainfall in the left-bank Ganga valley (see Fig. 2(a)). The valley of Brahmaputra alluvial plains is narrow compared to that of Ganga (Fig. 2(b)), highlighting the contrast in valley width across the HFR. The average valley width between the parent channel of the Brahmaputra and the Himalayan front is ~67.5 km, nearly three times the distance (~182.5 km) between the parent channel of the Ganga and the Himalayan front (see Fig. 2(b) for details). The rivers flowing along the HFR represent different geomorphic units, characterized by their source areas; mountain-fed, foothills-fed, plains-fed, and mixed-fed (Sinha and Friend 1994, Sinha *et al.* 2010).

The flow energy of the Himalayan rivers varies largely with seasons. They are primarily sluggish and sparse during winter, transforming into rapid and abundant waterways during the monsoon. The intensive monsoon rainfall, in contrast to the winter rainfall/precipitation, in Ganga and Brahmaputra regions (Datta and Singh 2004, Patel *et al.* 2021) is the key to the flow variations of the Himalayan rivers. These flow variations control the processes of sediment flux, aggradation, and degradation of the rivers of the HFR (Sinha 2005, Sinha *et al.* 2019). Besides meandering and braided rivers, straight and anastomosing river sections also feature the HFR. These distinctions in channel patterns can be linked to the sizes of the rivers and their flow energy transition near foothills. It is noteworthy that, based on Integrated Mission for Sustainable Development (IMSD), National Remote Sensing Agency (NRSA) guidelines, the slope of the Himalayan River basins shifts from strong and very steep (10 to >35%) in the hills to moderate and nearly level (0–10%) in the plains (Ramakrishnan *et al.* 2009 and the reference therein) (Fig. 2(c)). It leads to the flow energy transition of the Himalayan rivers near the foothill region and controls their channel patterns.

The Himalayan foreland region forms one of the largest alluvial basins in the world. The alluvial tract is mainly created by deposition of sediment generated in the Himalayas. The sediment depths to the basement rock vary significantly across the HFR (Dasgupta *et al.* 2000), reflecting lows and highs in the basement configuration. Researchers linked the basement configuration with the morpho-dynamics of rivers in the region (Lahiri and Sinha 2014, Borgohain *et al.* 2017). Another crucial geological feature of the Himalayas is its major thrusts across the mountain (see Fig. 3). The presence of thrusts and faults triggers regular earthquakes. These earthquakes have the potential to generate hefty sediment, affecting the morphology of the proximal rivers at a local and regional scale. Researchers reported such morphological changes in the Brahmaputra and its tributaries due to high sedimentation followed by the great Assam earthquake of 1950 (Goswami 1985, Lahiri and Sinha 2012).

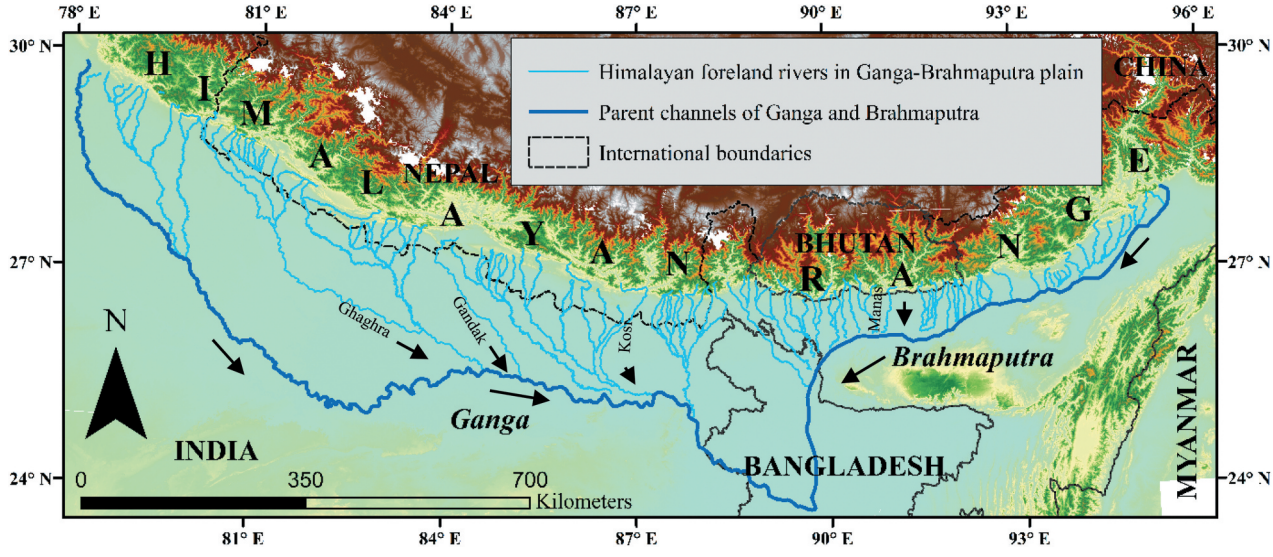


Figure 1. Study area map. It shows the Himalayan foreland rivers, across Ganga-Brahmaputra alluvial plain, considered in this study. The black arrows show the flow direction of rivers. Shuttle Radar Topography Mission (SRTM) Digital Elevation Model (DEM) (30 m resolution) is used for this demonstration.

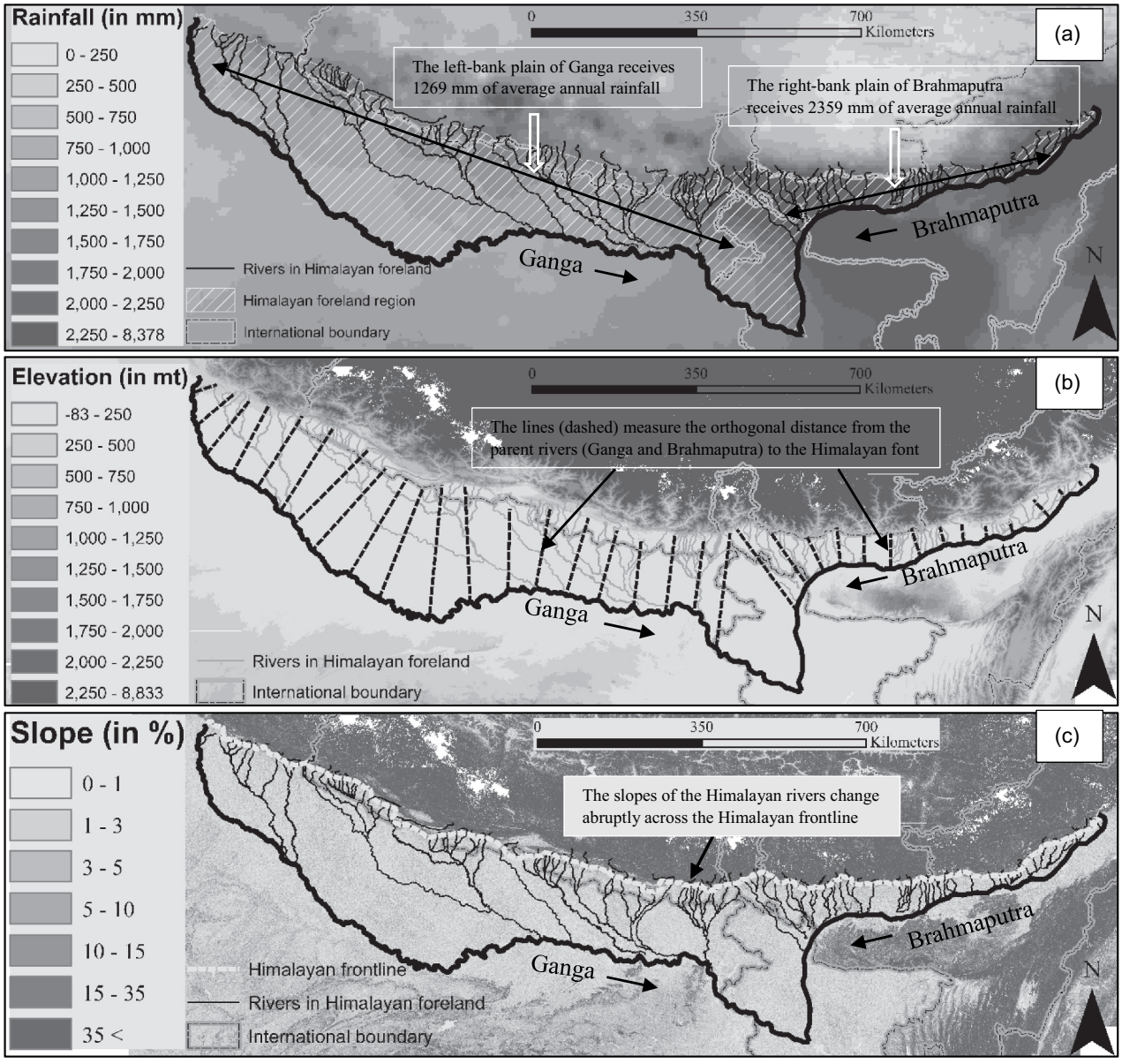


Figure 2. (a) Rainfall variations along the Himalayas and its foreland region. The greyscale gridded data (in the background) is Climate Hazards Group InfraRed Precipitation with Station (CHIRPS) average annual rainfall from 1990 to 2019. The CHIRPS data is used to measure the average annual rainfall of the left-bank plain of Ganga and the right-bank plain of Brahmaputra. (b) Expansion of Ganga and Brahmaputra valley along the Himalayan foreland region. The orthogonal lines (dashed) are used to measure the average valley width of Ganga and Brahmaputra to the north of their parent channels. Shuttle Radar Topography Mission (SRTM) Digital Elevation Model (DEM) (30 m resolution) is used to demonstrate the elevation distinction. (c) Change in slope of the rivers across the Himalayan front line. The slope map was generated from the SRTM DEM using ArcGIS software.

The flow directions of the Himalayan foreland rivers are controlled mainly by the surface tilts, the vegetation cover, and the orientation of the southern extension of the Himalayan block in the foreland region. However, we notice a consistency in aggraded-braided stretches along the foothills of several Himalayan foreland rivers that shift to downstream meandering (Sah *et al.* 2022). This shift in the channel pattern can be linked with the change in the flow energy of the rivers. When the rivers leave the hilly catchment and enter the flatter slope, their stream powers decrease, which leads to selective deposition of coarser grain, and creates a channel with low cohesion, resulting in a braided channel. The higher proportion of fine-grained sediments in the lower reaches of the rivers results in more cohesive floodplains supporting deeper and narrow channels (Valenza *et al.* 2020 and the references therein). The aggraded sections often form multi-channel flow characteristics, which facilitate switching channels from one to another. Such flow diversions between distributaries are triggered mainly by flood events. On the other hand, meandering stretches downstream to multi-thread portions often form levee breaches, as the initiation of sudden or sequential migration of the channel. Levee breaches and crevasse splays are common in the high-flow energy rivers of the HFR.

3 Data used

This study used Landsat images from 30 consecutive years (1990–2019) to document the chronological avulsion records

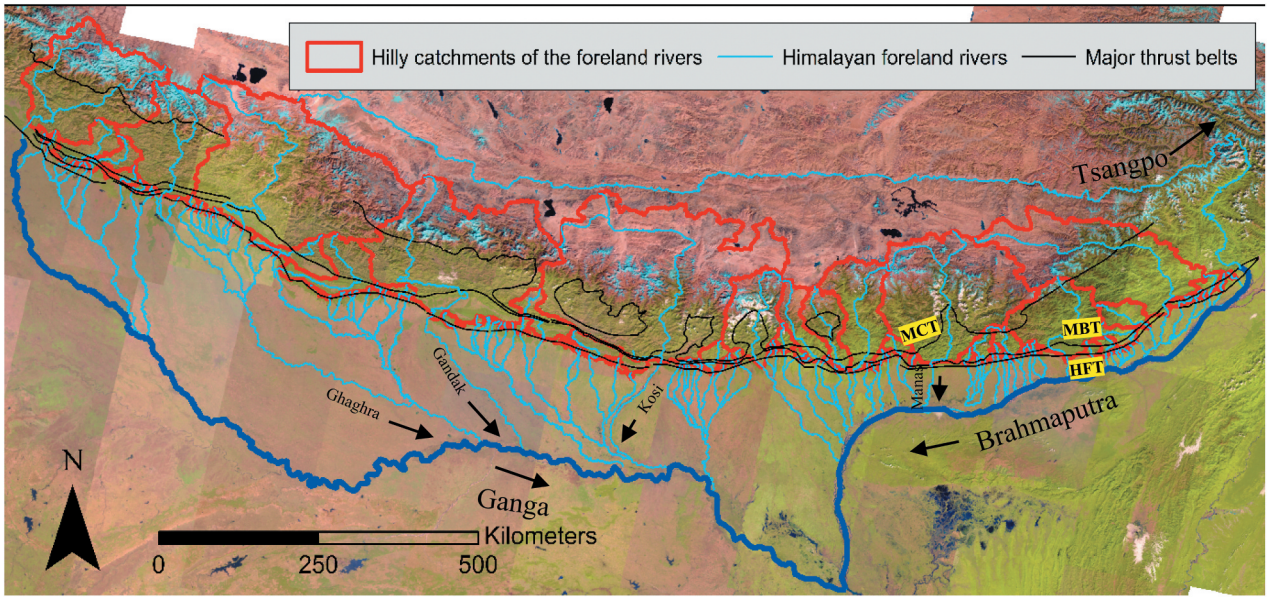


Figure 3. The hilly catchment areas and source regions of the rivers across the Himalayas. The thrust lines of the Himalayas are taken from the Bhukosh portal of the Geological Survey of India (http://bhukosh.gsi.gov.in/Bhukosh/MapViewer.aspx). The thrust lines of the region are indicated with the following abbreviations: MCT, main central thrusts; MBT, main boundary thrust; MFT, main frontal thrust. LandsatLook images of 2017 are used for this illustration.

in Himalayan foreland rivers (Table 1). Considering the large extent of the study area, acquiring cloud-free data for a year under evaluation is sometimes non-feasible. We considered the images of contiguous months of successive years in such cases. Floods are the most crucial trigger for river avulsion (Jones and Schumm 1999). Therefore, to document all possible avulsion activities, images of subsequent low-flow periods (separated by yearly flood seasons) were considered (Sah and Das 2018). When fingerprints proved insufficient for avulsion consideration, we used Landsat images taken during and immediately after monsoon periods for avulsion verification.

The names of the rivers were collected from topographical maps and published reports. The physiographic and climatic distinctions along the foreland region were evaluated using Shuttle Radar Topography Mission (SRTM) Digital Elevation Model (DEM) (30 m resolution) and Climate Hazards Group InfraRed Precipitation with Station (CHIRPS) rainfall data. SRTM DEM, along with Sentinel 2 and Google Earth Pro, was used for hilly catchment delineation of the rivers considered in this study. We used Landsat and Sentinel 2 imagery to identify different morphological (aggraded/braided, transitional, and meandering) reaches of the rivers.

4 Methods and approaches

We identified avulsion events from 110 rivers spread over the HFR (Table 2; Supplementary material 1, Table S1). As a result, rivers of various sizes originating in the upper, lower, and foothill regions of the Himalayas were included.

False Colour Composite (FCC) images were prepared for the HFR using Landsat and Sentinel 2 imagery. For this purpose, Near Infrared (NIR), red, and green spectral channels are used in the Geographic Information System (GIS) environment. The topographical maps were georeferenced using the geographical coordinate system with the WGS 84 datum. Following basic definitions, the abrupt relocations of channels are identified as river avulsions (Slingerland and Smith 2004, Coles and Klingeman 2014). We only include avulsions where the dominant flow is transferred to the avulsion channel. It consists of full and partial avulsions. A full avulsion is one in which all flow is transferred out of the parent channel, whereas a partial one occurs when only a portion of the flow is transferred (Slingerland and Smith 2004, Stouthamer 2014 and the reference therein). Our avulsion data do not contain the movements in the braided channels and the meander cuts (the details of the considered avulsion are given in the Supplementary material 1, Table S1).

The Himalayan foreland rivers also form anastomosing networks. Switching of major flow in such anastomosing networks cannot be categorized as a typical avulsion. Despite this, to add to the perspective of this study, flow migrations in multi-channel networks were also considered. Switching the dominant flow of anabranches in such complex morphologies (anastomosing) is the primary criterion for deciding flow migration activities.

We identified 286 river avulsions across the HFR. The novel avulsion dataset thus created is further utilized to assess the distribution of the events across the study region. We evaluated the avulsion distribution by plotting the identified avulsion events in the GIS platform. It also assisted us to locate the avulsion-affected areas in the HFR.

We delineated the hilly catchment areas of the rivers using SRTM DEM. While SRTM DEM was sufficient to delineate the majority of the watersheds, it is not enough to draw a definite watershed boundary for a few watersheds that originate in the Sub-Himalayan region. We assisted the watershed identification process with Sentinel 2 and Google Earth Pro in such cases. We identified the source regions of the rivers considered in this study. For this purpose, the major Himalayan thrusts, i.e. Main frontal thrust (MFT), Main boundary thrust (MBT), and Main central thrusts (MCT), are taken from the shape file available at the

Table 1. The chronological dataset used to identify the river avulsions across the Himalayan foreland region. The years of the dataset are presented in three different text fonts: regular, bold, and italics. The regular font indicates the Thematic mapper (TM), bold indicates the Enhanced Thematic Mapper Plus (ETM+), and italics indicats the Landsat Operational Land Imager/Thermal Infrared Sensor (OLI/TIRS) images.

	Path/row	Years
Landsat scenes	135/41	1991(2),1992,1993,1994,1996,1997(2),1999,2000(2),2004(2),2006(2),2008(2),2010,2011; **2002,2003,2011,2013**; *2014(2),2015,2017(2),2018,2020*
	136/41	1990,1991,1992,1993,1994,1996(2),1997,1998,1999,2000,2004(2),2006(2),2008(2),2010(2),2011; **2001,2002,2012**; *2014(2), 2015,2016,2017,2018,2019*
	136/42	1991,1992,1993(2),1994,1996,1997,1998(2),2000,2001,2004,2005,2006,2007,2008,2009,2010(2),2011; **2002(2),2013**; *2013,2014,2015,2016,2017,2018,2020*
	137/41	1991(2),1992,1994(2),1995,1996,1998,1999(2),2000,2003,2004,2006(2),2008(2),2010(2); **2001,2002,2011,2012**; *2013,2015(2)2016,2017,2018,2019*
	137/42	1991,1992(2),1993,1994,1995,1996,1998,1999(2),2000,2003,2004,2005,2007,2008,2009,2010(2); **2002(2),2011,2012**; *2013,2015(2),2016,2017,2019(2)*
	138/41	1990,1991,1992,1993,1994,1996(2)1997,1998,1999,2000,2003,2004,2005,2006,2008(2),2010,2011(2); **2001,2002,2013**; *2014,2015(2),2016,2017,2018,2019*
	138/42	1990,1991,1992,1933,1995,1996(2),1997,1998,1999,2001,2004(2),2005,2006,2008,2009(2),2010,2011; **2001,2002,2013**; *2014,2015(2),2016,2017,2018,2019*
	139/41	1990,1991,1993,1994(2),1996(2),1997,1998,1999,2000,2003,2004,2005,2006,2008(2),2010(2),2011; **2001,2002,2013**; *2013,2014,2015,2016,2017,2018,2019*
	139/42	1990,1991,1992,1993,1994,1996(2),1997,1999(2),2000,2003,2005,2006,2008(2),2009,2010,2011; **2001,2002,2012**; *2013,2014,2015,2016,2017,2018,2019*
	140/41	1991,1992(2),1993,1994,1995,1996,1997,1998,1999,2000,2003,2004,2005,2006,2008(2),2009,2010; **2002(2),2011,2012**; *2013,2014,2015,2016,2017,2018,2019*
	140/42	1991,1992(2),1994(2),1995,1996,1998(2),1999,2001,2003,2004,2005,2006,2008(2),2009,2010; **2002(2),2011,2012**; *2013,2014,2015,2016,2017,2018,2019*
	141/41	1991(2),1992,1993,1995(2),1996,1998(2),1999,2000,2003,2004,2005,2006,2008(2),2009,2010,2011; **2001,2002,2012**; *2013,2014,2015,2016,2017,2018,2019*
	141/42	1991(2),1992,1993,1994,1995,1996,1997,1998,1999,2000,2004,2005,2006,2008(2),2009,2010,2011; **2001,2002,2003,2012**; *2013,2014,2015,2016,2017,2018,2019*
	142/41	1991(2),1992,1993,1994,1995,1996,1998,1999,2003,2004,2005,2006,2008(2),2009,2010,2011; **2000,2001,2002,2012**; 2013,2014,2016(2),2017,2018,2019
	142/42	1991(2),1992,1993,1994,1995,1996,1998,2003,2004,2005,2006,2008(2),2009,2010; **1999,2000,2002,2003,2011,2012**; 2013,2014,2015,2016,2017,2018,2019
	143/41	1990,1991,1992,1993,1994,1995,1996,2004(2),2005,2006,2008,2009,2010,2011; **1999,2001(2),2002,2007,2012**; *2013,2014,2015,2016,2017,2018,2019*
	144/40	1991(2),1992,1993,1994,1995,1996,1998(2),2001,2008,2009,2010; **1999,2002(2),2003,2004,2005,2006,2007,2011,2012**; *2013,2014,2015,2016,2017,2018,2019*
	144/41	1991(2),1992,1993,1994,1995,1996,1998(2),1999,2004,2008,2010(2); **2000,2001,2002,2003,2005,2006,2007,2011,2012**; *2013,2014,2015,2016,2017,2018,2019*
	145/40	1991,1992,1993(2),1994,1995,1996,1997,1998,2008,2009,2010,2011; **1999,2000,2001,2002,2003,2004,2005,2006,2007,2012**; 2013,2014,2015,2016,2017,2018,2019
	145/41	1990,1992,1993(2),1994,1995,1996,1997,1998,2000,2008,2009,2010,2011; **1999,2001,2002,2003,2004,2005,2006,2007,2012;** *2013,2014,2015,2016,2017,2018,2019*
	146/39	1991,1992(2),1993,1994,1995,1996,1998(2),2000,2008,2009,2010; **2000,2001,2002,2003,2004,2005,2006,2007,2011,2012**; *2013,2014,2015,2016,2017,2018,2019*
	146/40	1991,1992(2),1993,1994,1995,1996,1997,1998,2008,2009,2010; **1999,2000,2001,2002,2003,2004,2005,2006,2007,2011,2012**; *2013,2014,2015,2016,2017,2018,2019*

Table 2. Avulsion activities in the rivers of Himalayan foreland region (HFR).

Rivers[1]	Number of avulsion events	Category[2]	Rivers[1]	Number of avulsion events	Category[2]
1. Remi	1	Rare	56. Ratua	0	Rare
2. Dikari	8	Common	57. Bakra	3	Occasional
3. Simen	6	Common	58. Dash	0	Rare
4. Dimou	15	Frequent	59. Chisang	0	Rare
5. Gai	13	Frequent	60. Lohondra	2	Occasional
6. Jiadhal	16	Frequent	61. Keshalia	2	Occasional
7. Subansiri	1	Rare	62. Kosi	1	Rare
8. Ranganadi	6	Common	63. Trijuga	7	Common
9. Dikrong	1	Rare	64. Bhuthi Balan	9	Common
10. Pichala	13	Frequent	65. Kamla	14	Frequent
11. Sessa	17	Frequent	66. Yamuni	6	Common
12. Solengi	18	Frequent	67. Bighi	2	Occasional
13. Kukurjan	9	Common	68. Bagmati	7	Common
14. Brahmajan	11	Frequent	69. Lal Bakaiya	0	Rare
15. Burai	0	Rare	70. Pashah	3	Occasional
16. Bargang	0	Rare	71. Sarsiwa	8	Common
17. Jiabhareli	0	Rare	72. Bherang	2	Occasional
18. Belsiri	3	Occasional	73. Sikta	5	Occasional
19. Sirajuli	3	Occasional	74. Uria	1	Rare
20. Panchnoi	1	Rare	75. Kartaha	0	Rare
21. Rowta	0	Rare	76. Pandai	0	Rare
22. Dhansiri	1	Rare	77. Buri Gandak	1	Rare
23. Golandi	6	Common	78. Gandak	0	Rare
24. Mangaldai	1	Rare	79. Rohini	0	Rare
25. Noa	4	Occasional	80. Tinau	0	Rare
26. Nanai	3	Occasional	81. Dano	0	Rare
27. Kulsi	0	Rare	82. Banganga	0	Rare
28. Puthimari	3	Occasional	83. Surahi	0	Rare
29. Baralia	2	Occasional	84. Arrah	0	Rare
30. Nona	8	Common	85. Rapti	1	Rare
31. Pagladia	3	Occasional	86. Dundawa	0	Rare
32. Manas	1	Rare	87. Man	0	Rare
33. Kanamakra	0	Rare	88. Babai	0	Rare
34. Aie	1	Rare	89. Ghaghra	1	Rare
35. Chamapamati	3	Occasional	90. Patharia	0	Rare
36. Gaurang	1	Rare	91. Karha	3	Occasional
37. Tipkai	1	Rare	92. Kandra	0	Rare
38. Bhamka	0	Rare	93. Kateni	3	Occasional
39. Sankosh	1	Rare	94. Ghurah	0	Rare
40. Raidak	0	Rare	95. Khutia	0	Rare
41. Gagadhar	1	Rare	96. Mohana	0	Rare
42. Nonai	0	Rare	97. Suheli	4	Occasional
43. Dima/Garam	0	Rare	98. Choundhar	2	Occasional
44. Kaljani	2	Occasional	99. Sharda	0	Rare
45. Torsa	0	Rare	100. Jagbura	0	Rare
46. Angrabhasa	1	Rare	101. Kamin	0	Rare
47. Jadhaka	0	Rare	102. Deoha	2	Occasional
48. Neora	0	Rare	103. Gaula	1	Rare
49. Chel	1	Rare	104. Kosi	3	Occasional
50. Tista	0	Rare	105. Dhela	2	Occasional
51. Mahanadi	0	Rare	106. Phika	1	Rare
52. Chenga/Manja	0	Rare	107. Dhara	1	Rare
53. Mechi	0	Rare	108. Ramganga	0	Rare
54. Biring	1	Rare	109. Khoh	1	Rare
55. Kankai	0	Rare	110. Malin	1	Rare

[1]The rivers are listed from east to west along the Ganga-Brahmaputra plain.
[2]A generic categorization is done to group the avulsion events of the study rivers, i.e. <2 events = rare; 2–5 events = occasional; 6–10 events = common; >10 events = frequent.

Bhukosh portal of the Geological Survey of India (http://bhukosh.gsi.gov.in/Bhukosh/MapViewer.aspx) (see Fig. 3). Based on the thrust lines, the Sub-Himalayas, Lesser Himalaya, and Higher Himalaya regions are considered (Roy 2014). Then the source regions of the avulsion-affected river are identified (Fig. 3).

The distance from the avulsion site to the Himalayan foothills is measured along the channel-belt centrelines of the rivers. In HFR, river path adjustments are common in several rivers. Therefore, we needed to demarcate the channel belt of the rivers for each avulsion year. Each river is classified as comprising aggraded/braided, transitional, or meandering reaches based on the channel pattern along its longitudinal span. The upper river sections with aggraded beds and/or multiple threads are classified as braided reach. The lower sinuous bank lines with a single thread are considered meandering reaches. The meandering stretches sometimes form more than one channel. In such cases, they are distinguished by their tortuous channel patterns. And the middle section where the rivers transform

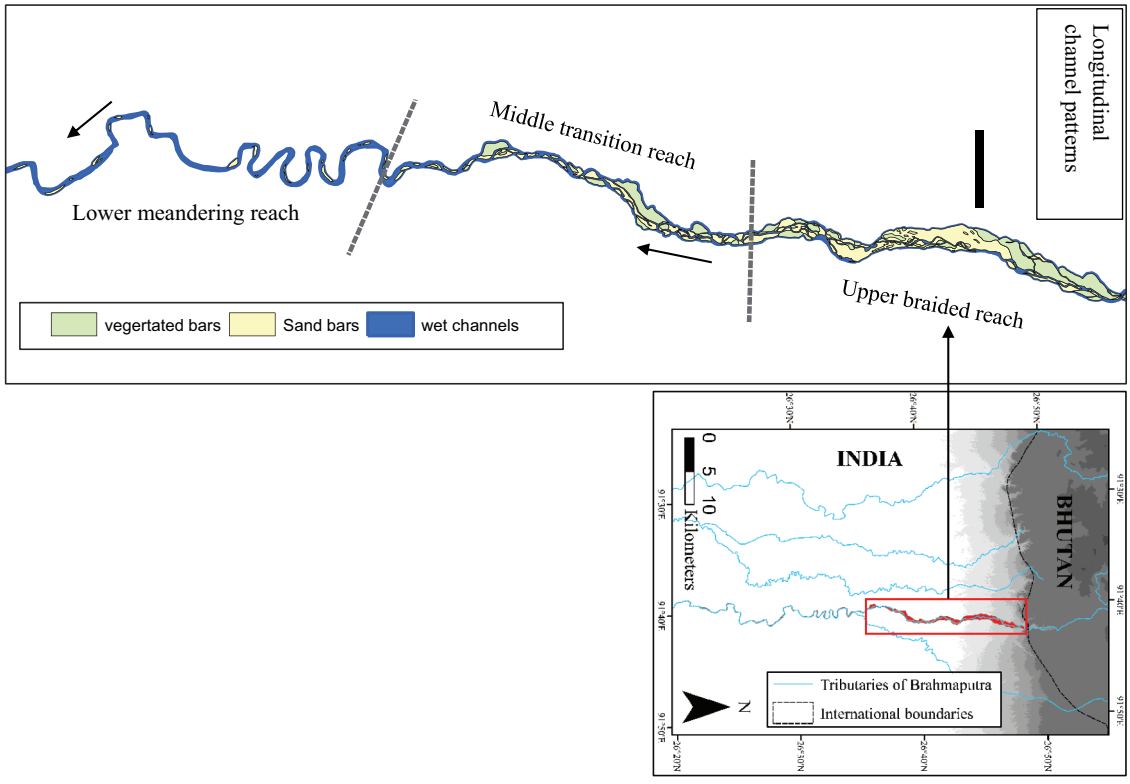


Figure 4. The longitudinal shift in channel patterns of the Puthimari River. The channel planform features are delineated from Sentinel 2 images of 2019.

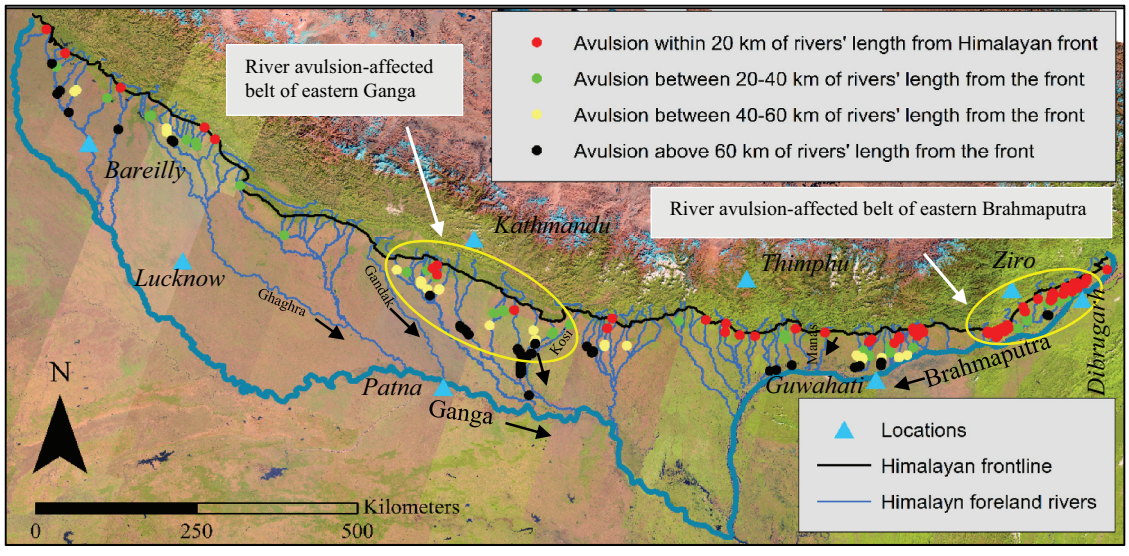


Figure 5. Distribution of river avulsions across the Himalayan foreland region (HFR). The circles represent the two active belts of river avulsions in the eastern Ganga and Brahmaputra regions. LandsatLook images of 2017 are used for this illustration.

from braided to meandering sections is identified as transitional reach (in the sense of Fuller *et al.* 2013, Edmonds *et al.* 2016, Valenza *et al.* 2020) (Fig. 4).

The CHIRPS dataset is used to assess the rainfall pattern across the HFR. For this purpose, an average annual rainfall map was prepared using gridded rainfall data from 1990 to 2019 (Fig. 2(a)). We used the average rainfall map to interpret the spatial variation in rainfall along the foreland. SRTM DEM was utilized to compute the valley width of the foreland region (Fig. 2(b)).

Interviews with the local residents near the avulsion-affected rivers were conducted to supplement our observations. The interviews included inquiries on (a) the effect of the 1950 Assam earthquake on eastern Brahmaputra tributaries and (b) the tributaries' morphological changes in recent decades. Members of the elderly age group (60–80+ years old) were included in the interviews as they are observers of the post-1950 earthquake scenario and the past morphological changes in the rivers in the region. We collected photographic evidence as well during the field visit.

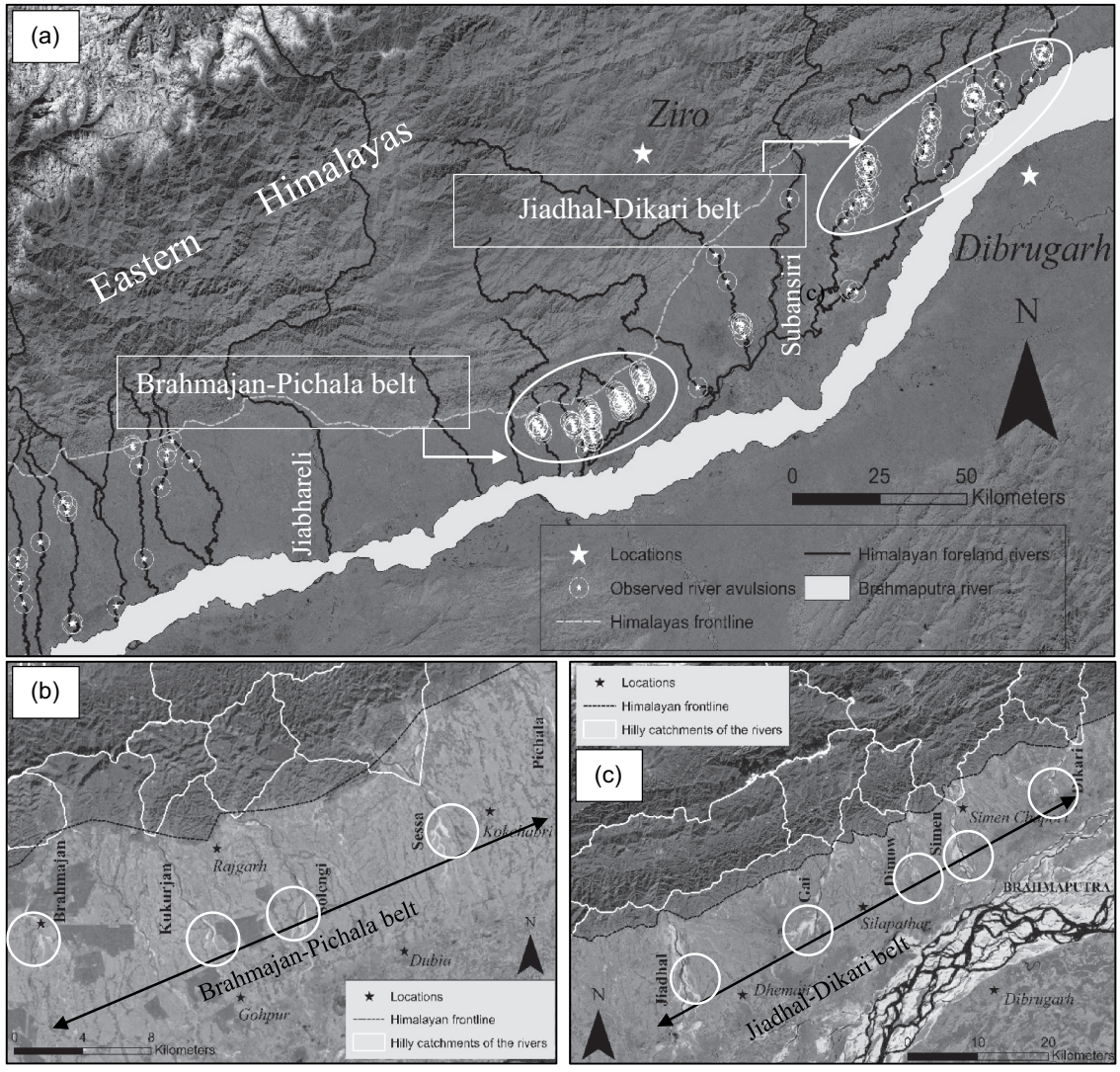


Figure 6. (a) Locations of Jiadhal-Dikari and Brahmajan-Pichala belts. Evidence of several avulsion scars (white circles) in the (b) Brahmajan-Pichala and (c) Jiadhal-Dikari belts highlights the dynamic nature of the rivers. Landsat images of the year 1998 are used to demonstrate the avulsion scars.

5 Results

5.1 Distribution of river avulsions in HFR

Figure 5 shows the distribution of avulsion events in the rivers of the HFR. We noted 19 rivers with frequent (>10 events) or common (6–10 events) avulsion activities along the foreland. They comprise more than 17% of the rivers considered in this study (Table 2). Most of the identified avulsions occurred in the eastern part of the Ganga and Brahmaputra plains (Table 2). In contrast, the western regions of both the Ganga and Brahmaputra have suffered limited avulsions.

We identify two major belts of river avulsions, in eastern Ganga and eastern Brahmaputra (Fig. 5). The eastern rivers of Ganga (e.g. Kamla, Bhuthi Balan, Trijuga, Bagmati) have shown a higher number of avulsion activities than the western ones (Table 2). In the last three decades, we recorded six rivers in the eastern belt with ≥ 6 avulsion events. Apart from these rivers, several ephemeral streams in the Ganga plains originate in the foothill regions. The ephemeral rivers disappear (do not have a distinct channel) into permeable sediments after flowing for a certain distance in a zone called *Bhabar* (a gently sloping coarse alluvial zone below the Sivalik hills). The smaller sizes and impermanent situation render the proper interpretation of their avulsion nature impractical. However, based on the scars of the brighter sediment splays, we can infer that those smaller rivers are dynamic.

Along the eastern region of the Brahmaputra plain, we observed several rivers with frequent avulsions (Fig. 6(a)). We identified the Jiadhal-Dikari belt (Fig. 6(c)) and the Brahmajan-Pichala belt (Fig. 6(b)). These belts drain seven rivers that each have more than 10 avulsion events (Table 2). Moreover, several small rivers (e.g. Fig. 7) in this eastern belt also displayed similar avulsion characteristics in the study period. This indicates that the region is one of the most river avulsion-prone belts in the HFR.

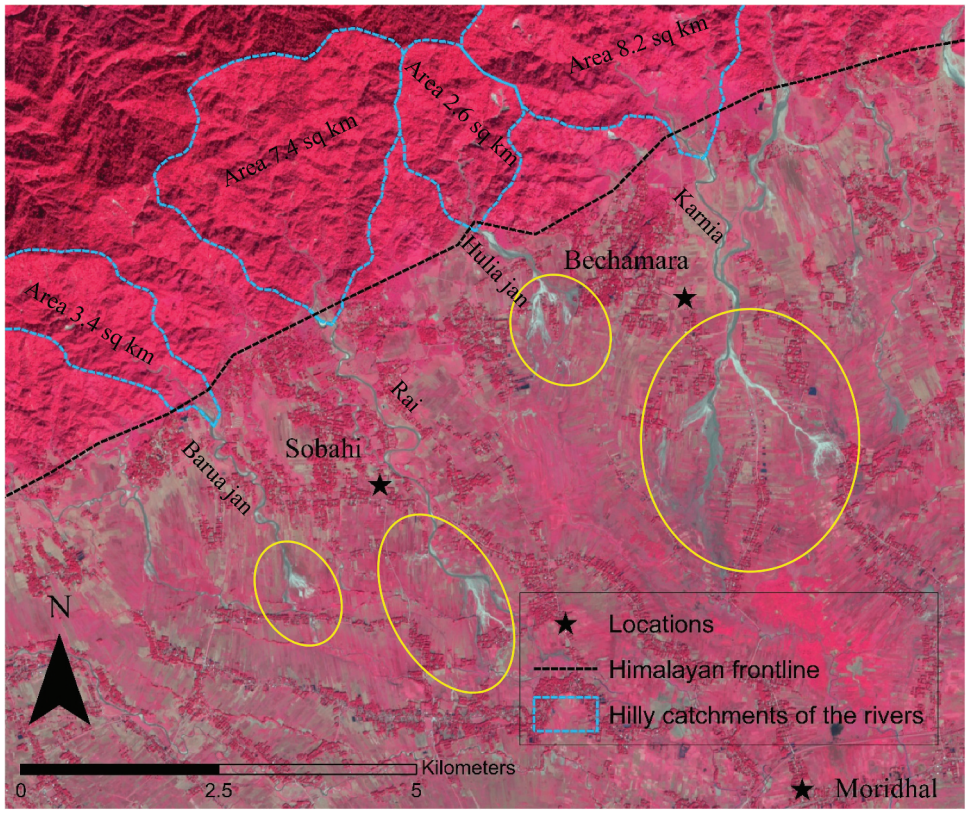


Figure 7. Avulsion scars (marked with circles) can be seen in the smaller rivers (of hilly catchment areas < 10 km^2) of the eastern Brahmaputra plains. These rivers lie between Jiadhal and Gai. The False Colour Composite (FCC) is prepared using Near Infrared (NIR), red, and green spectral channels of Sentinel 2 imagery for 2017.

Table 3. The catchment sizes and source region of origins of the avulsion-affected rivers (with six or more avulsion events in last three decades) in Himalayan foreland region (HFR).

Rivers	Number of avulsion events	Source regions of their origin	Hilly catchment areas (in m^2)
1. Solengi	18	Sub-Himalayas	26 063 311
2. Sessa	17	Sub-Himalayas	53 899 984
3. Jiadhal	16	Southern part of Lesser Himalayas	359 105 516
4. Dimou	15	Sub-Himalayas	63 000 804
5. Kamla	14	Lesser Himalayas	1 595 208 027
6. Pisola	13	Sub-Himalayas	16 549 009
7. Gai	13	Southern part of Lesser Himalayas	135 039 748
8. Brahmajan	11	Sub-Himalaya	15 052 017
9. Kukurajan	9	Sub-Himalayas	18 430 213
10. Bhuthi Balan	9	Sub-Himalayas	222 807 902
11. Dikari	8	Southern part of Lesser Himalayas	188 219 035
12. Nona	8	Southern part of Lesser Himalayas	25 591 152
13. Sariswa	8	Sub-Himalayas	27 332 925
14. Trijuga	7	Sub-Himalayas	45 109 729
15. Bagmati	7	Higher Himalayas	2 812 422 111
16. Ranganadi	6	Lesser Himalayas	2 243 850 091
17. Simen	6	Lesser Himalayas	769 815 929
18. Golandi	6	Sub-Himalayas	56 355 766
19. Yamuni	6	Sub-Himalayas	42 056 051

5.2 River sizes and frequency of avulsion

To quantify the frequency of avulsion in different-sized tributaries, we assessed hilly catchment areas and the regions of origin of the study rivers (Fig. 3). We found that avulsions are more common in smaller rivers. Nearly 80% of the avulsion-affected rivers (≥ 6 avulsion events) originate in or below the southern part of the lesser Himalayas (Table 3). All these active rivers have hilly catchment areas of less than 500 km^2 (Table 3).

5.3 Longitudinal distribution of river avulsions to the Himalayan foothills

We noted that avulsions often occurred in the reaches of tributaries proximal to the Himalayan front. More than 50% of the avulsion events occurred within a range of 0–20 km from the foothill region. Proximal river avulsions (to the Himalayan foothills) are a common feature of tributaries of Brahmaputra. Nearly 75% of the recorded avulsion events in tributaries of Brahmaputra lie within 20 km of the Himalayan

Table 4. Longitudinal distribution of the recorded avulsions along the rivers in Himalayan foreland region (HFR).

Distances of the identified river avulsions from Himalayan front (in km)	Number of river avulsion events	Number of avulsion events in the rivers of Brahmaputra plain	Number of avulsion events in the rivers of Ganga plain
<10	100	94	6
10–20	49	45	4
20–30	39	18	21
30–40	18	8	10
40–50	24	10	14
50–60	10	1	9
60–70	16	7	9
70–80	8	3	5
80–90	4	0	4
90–100	6	0	6
>100	12	0	12

Table 5. The distribution of the avulsions in the different morphological reaches of the rivers in Himalayan foreland region (HFR).

Classified morphological reaches of the rivers	Number of river avulsion events	Number of avulsion events in the rivers of Brahmaputra plain	Number of avulsion events in the rivers of Ganga plain
Braided	50	41	9
Transitional	127	102	25
Meandering	109	43	66

front (Table 4). However, in the Ganga plains, the number of avulsions is higher between 20 and 50 km from the foothills.

5.4 Avulsion distribution among different morphologies

Observations of avulsion events along different morphologies of rivers along the HFR are shown in Table 5. The figure shows that the meandering and transition reaches of the rivers have suffered most of the avulsion in the last three decades. However, a difference in avulsion distribution is noticed in Brahmaputra and Ganga plains. In the Brahmaputra, avulsions are common in the transition zone (>50%), whereas the lower meandering section has suffered the highest avulsions in the tributaries of Ganga (Table 5). We also note that the degree of morphological changes of the rivers in their transitional reaches varies largely across the HFR. Most rivers have a gentle transition from braided to meandering channel patterns. The others have a rapid shift in morphology along their transition reaches (e.g. Jiadhal, Gai, Trijuga, Yamuni). Examples of gentle and rapid transitions in morphology are given in Fig. 8. Compared to Balaria, Puthimari, and Kulsi, Jiadhal has a wide braided channel upstream that switches to a narrow meandering channel along the transition zone. Across the transition zone, the change in the river width of Jiadhal is considerably high compared to those of Baralia, Puthimari, and Kulsi (Fig. 8(c)). Rivers with such rapidly shifting transitional reaches have suffered more avulsions. Nodal avulsion (that is, avulsion limited to particular stretches) is also noticed in such rivers.

6 Discussion

We find that river avulsions are not occurring evenly throughout HFR but are clustered in eastern parts of the Ganga and Brahmaputra plains. Two river belts, i.e. Jiadhal-Dikari and Brahmajan-Pichala, are among the most avulsion-affected areas in the HFR. Considering the dynamic nature of the rivers in these active belts of the Brahmaputra and the long association of the authors with the region, the drivers are further explored.

The dynamic rivers in the Jiadhal-Dikari belt are closer to the epicentre of the great Assam earthquake of 1950. Researchers believe that the Assam earthquake has impacted several rivers of Brahmaputra (Goswami 1985, Lahiri and Sinha 2012). The isoseismal of the earthquake indicates a large rupture in the hilly catchments of the rivers of the Jiadhal-Dikari belt (Poddar 1950, Sah *et al.* 2022). Corona photographs of December 1961 are explored to assess the post-earthquake sedimentation in the rivers of the Jiadhal-Dikari belt. The Corona photographs are one of the earliest sources of aerial information after the 1950 Assam earthquake that can be utilized for such geomorphic investigation. We notice sand splay deposits, analogous to large ruptures in the hilly catchments during the 1950 earthquake, along the foothill region of the rivers (alluvial fan) (Fig. 9).

Field photographs and the narratives of the local residents supplement our observation. Sah *et al.* (2022) interviewed the locals and reported high earthquake-induced sedimentation in the northern tributaries of the Brahmaputra proximal to the 1950 earthquake. Our field study corroborates this observation. We noted that the natives of the region unanimously agreed on the extensive sedimentation and river course changes following the well-known earthquake. During our field visit, we noticed several dead trees within the Jiadhal River bed (Fig. 10). Those trees potentially testify to massive sedimentation along the Jiadhal River corridor after the 1950 Assam earthquake. The aftermath sedimentation buried those trees. The buried trees come out when Jiadhal scours its channel through those depositional areas. This can be confirmed from the narratives of the locals. They often find buried trees in this region while digging a new pond. Field narratives, photographs, and depositional features suggest massive sedimentation along the rivers following the 1950 Assam earthquake, which has significantly affected their avulsion behaviour.

The rivers along the Brahmajan-Pichala belt, lying in the narrow alluvial region between Mikir and Dafla hills, are relatively small. We noticed that these rivers have non-incised channels (Fig. 11). To investigate whether any morphological transformation of the rivers has taken place, we compared their present morphology to that in Corona photographs (1962) and topographical maps (1962–1963) (Fig. 12; Supplementary material 2, Fig. S1). We identified that the rivers in the past were flowing through narrower and more sinuous reaches than their

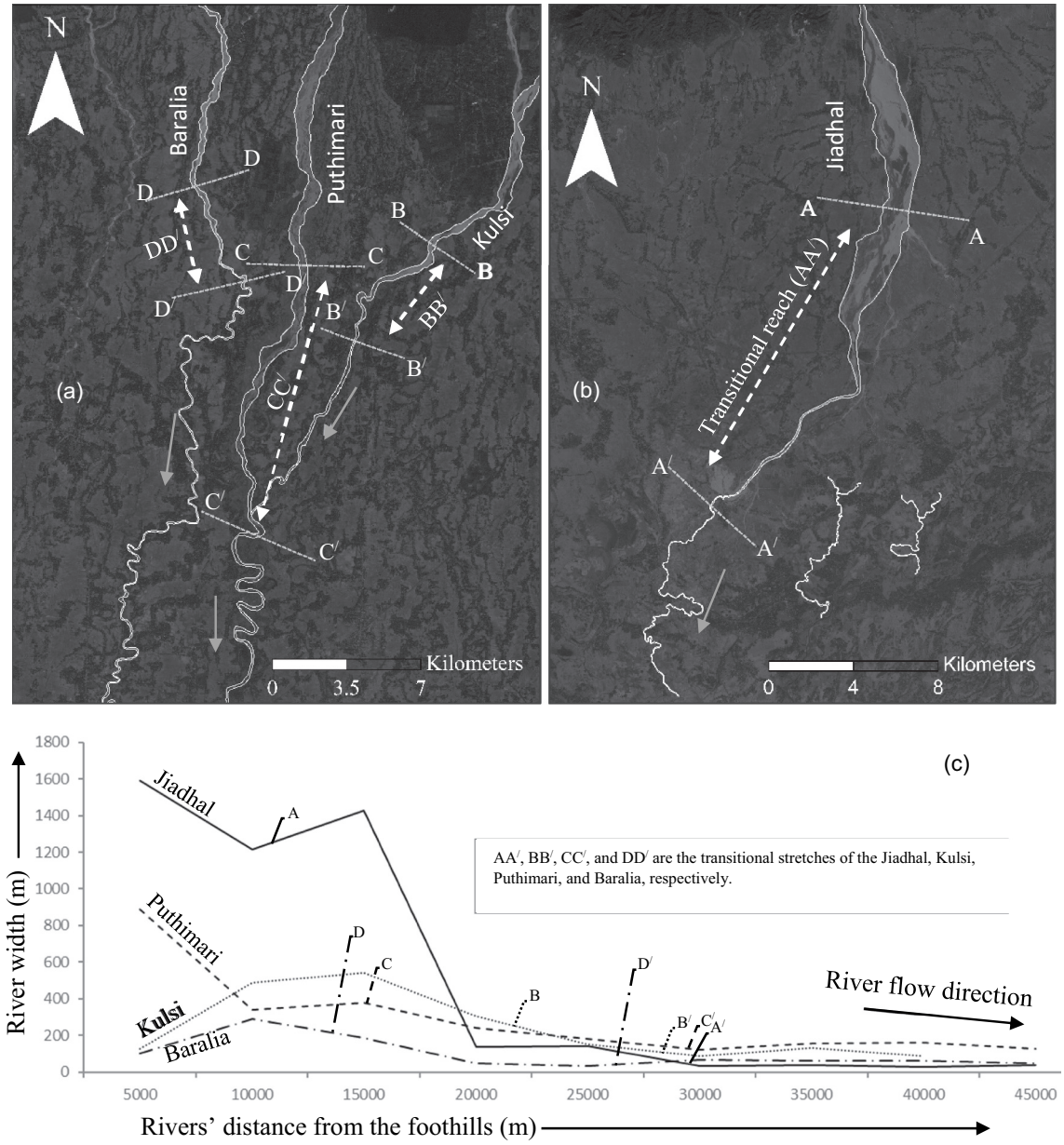


Figure 8. A gentle shift in channel pattern along the transition zone of Baralia, Puthimari, and Kulsi is noticed (a). However, the change is rapid along the transition zone of Jiadhal (b). Jiadhal has a wide braided channel upstream that rapidly switches to a narrow and meandering channel along the transition zone. The widths of the rivers are measured at an interval of 5000 m from the foothills (see Supplementary material 1, Table S2). The graphical representation of the downstream changes in the widths of Baralia, Puthimari, Kulsi, and Jiadhal show marked variations (c). The width of Jiadhal changes rapidly compared to Kulsi, Puthimari, and Baralia. White lines show the bank lines of the rivers. The 2019 greyscale image of Sentinel 2 (red channel) is used for this demonstration.

present courses. The locals affirmed such morphological adjustments in the rivers. They insisted that in the 1950s, the rivers in the region were flowing through relatively narrow and incised channels. If we explore the potential factors that can result in the morphological change of these rivers in such a short period (in decades), the great 1950 Assam earthquake and the changes in land cover seemed to be the crucial ones. However, looking at the Corona photograph, we can ascertain that the effect of the 1950 Assam earthquake on the rivers along the Brahmajan-Pichala belt is limited. Instead, locals of the region claimed that deforestation is one of the critical factors that has resulted in the morphological changes of the rivers. Extensive deforestation in the area can be noticed in the present images compared to Corona Photographs (Fig. 12; Supplementary material 2, Fig. S2). The upper stretches of the rivers were protected by forests. The locals also stressed that extensive deforestation in the recent past and changes in river morphology had altered the avulsion behaviour of the rivers. Such deforestation can lead to a higher erosion rate in basins, increasing the sediment load of the associated rivers (Restrepo *et al.* 2015). The recent transformation (into the non-concise channel) of the rivers in the Brahmajan-Pichala belt is conceivably due to larger sediment loads in their channels triggered by the deforestation in the region. Their transformed aggraded channels have reduced water- and sediment-carrying capacities, thus facilitating regular avulsions. Both field narratives and our observations indicate that the rivers have transformed into non-incised ones, contributing to their avulsion behaviour.

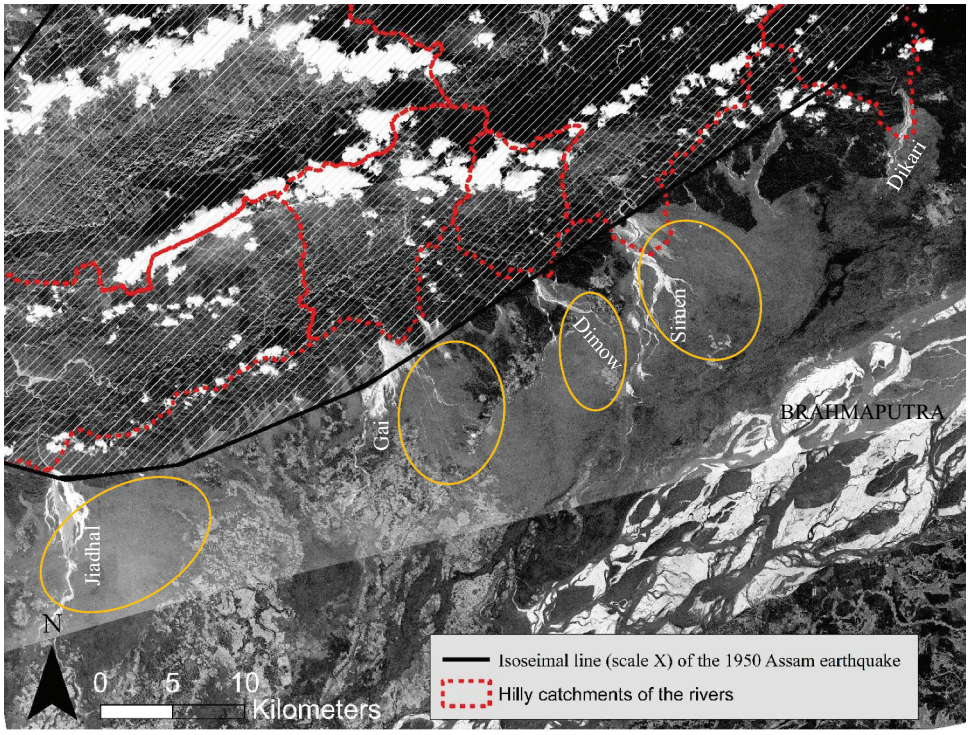


Figure 9. Corona photograph of the year 1961. In the image, sand splay deposits on the alluvial fan (marked with circles) are noticed along the rivers lying in the Jiadhal-Dikari belt. The hilly catchments of the rivers fall in largely affected areas (isoseismal of scale X, Poddar 1950) of the 1950 Assam earthquake.

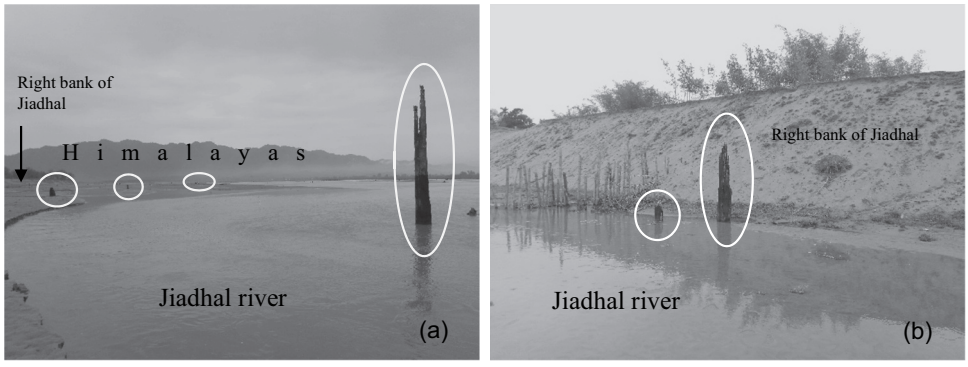


Figure 10. (a) Remnants of the trees in the riverbed of Jiadhal. (b) The buried tree emerges when the river erodes its banks. In the photographs, the white circles show the tree remnants.

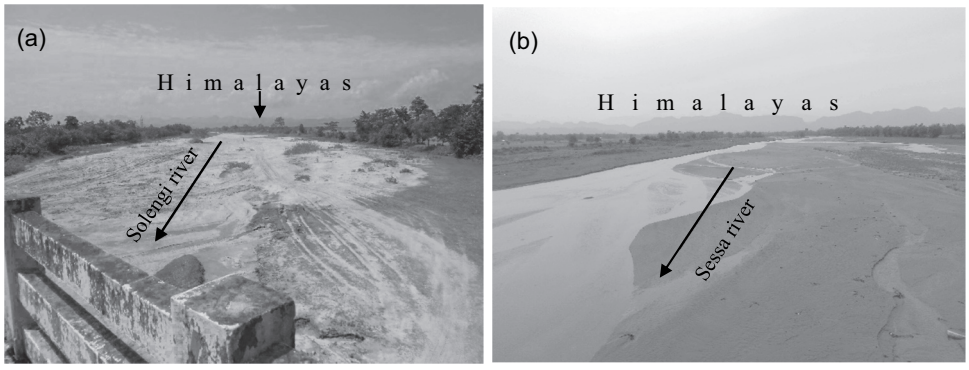


Figure 11. The aggraded bed of (a) Solengi and (b) Sessa rivers in the eastern Brahmaputra plains.

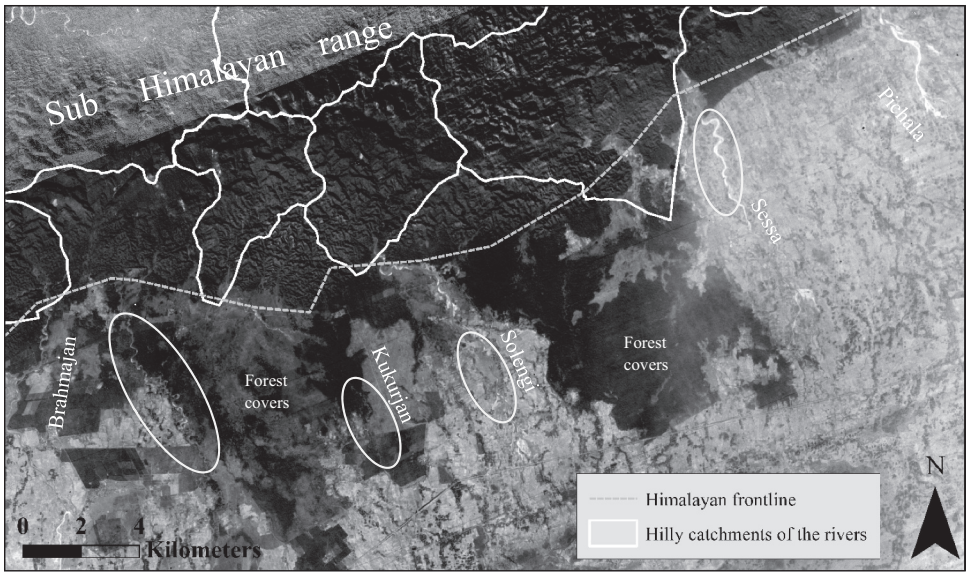


Figure 12. Corona photograph of the year 1962. It shows a large forest cover along the stretch of the Brahmajan-Pichala belt. Stretches of several rivers were meandering (marked with circles), straightened over the last few decades.



Figure 13. A photograph taken near the Sessa bridge (Simaluguri). The embanked river Sessa can be seen flowing through a channel of higher elevation compared to its adjacent floodplain.

Comparing the frequency of avulsion in different-sized rivers along HFR, we noticed that small rivers originating in sub-Himalayan regions are more susceptible to avulsion activities. During our field visit, we noted that the dynamic stretches of the small rivers of Brahmaputra do not have an incised channel (e.g. Fig. 11). Reports suggested that some of them flow through a higher elevation channel/belt than their neighbouring floodplains (Borgohain *et al.* 2016, Sah *et al.* 2022). Sessa is such a river that we noted during our field visit (Fig. 13). Such aggraded rivers have less channel capacity and gradient advantage for avulsion activities (Makaske 2001, Slingerland and Smith 2004).

Another critical factor is the rapid morphological change in the smaller rivers in their transitional reaches. We measured the widths of the tributaries of Brahmaputra to identify the ones experiencing such rapid changes. We noted that six rivers (Dikari, Dimou, Gai, Jiadhal, Sessa, and Solengi) decrease in width by more than 10-fold (within a 10-km reach) downstream of the foothills (Supplementary material 1, Table S2). The noted changes are the highest amongst the tributaries of Brahmaputra. Moreover, those rivers fall within the Jiadhal-Dikari and Brahmajan-Pichala belts. And rivers having rapidly shifting transitional reaches have suffered more avulsions. Thus, the aggraded bed and rapid morphological transition of the smaller rivers have contributed to their frequent avulsions in the HFR.

Alluvial stratigraphy in foreland basins generally displays a stratigraphically downward shift from channel-

dominated sandy facies to floodplain-dominated muddy facies (Valenza *et al.* 2020). This is basically due to changes in the depositional environments of the rivers from foothills to downstream floodplain regions. The contrast in channel pattern change (Fig. 8(b)) and stability can be seen in Jiadhal, one of the most active rivers in the HFR. The lower meandering stretches of the river are relatively stable compared to the upper braided and transitional reaches. A similar pattern is noticed along HFR: i.e. avulsion events are higher in the transitional reaches of the rivers (and the adjacent braided and meandering sections). We also noted nodal avulsions (avulsions limited to particular stretches) along the transitional reaches of a few rivers. Nodal avulsions are mainly noticed in the rivers that have an abrupt shift in channel pattern along their transitional reach. Examples are the eastern Himalayan rivers (e.g. Jiadhal and Gai), which form alluvial fans and shift their channel width rapidly. Recurrent river avulsions are reported in alluvial fans (Assine 2005, Chakraborty *et al.* 2010). In this study, especially the toe regions of the alluvial fans (or the sandy facies to muddy facies transition areas) have shown nodal avulsions. This is because of the sediment imbalance along the transition zones of the rivers and their relative capability to carry the water and sediment.

This work focused on modern river avulsions (1990–2019) and integrated 286 avulsion events along HFR, thus offering an opportunity to recalibrate our observations with global river avulsion records. Works based on modern and historical observations across various global fluvial systems suggest multiscale avulsion frequencies for rivers. The avulsion frequencies of the lower Mississippi River in the delta region and the Klip River reach near Memel varied from nearly 1000 years to several thousand years (Aslan *et al.* 2005, Tooth *et al.* 2007). With relatively higher avulsion frequencies, the lower Saskatchewan River and lower reach of the Tshwane River changed their courses at an interval between a century and a millennium (Morozova and Smith 1999, Larkin *et al.* 2017). In the Kosi River along the Himalayan foreland and the lower Yellow River in its deltaic region, the avulsion frequencies range from about a decade to a few decades (Wang and Liang 2000, Slingerland and Smith 2004 and the reference therein). Chronological investigations based on recent satellite images suggest that several rivers in the southern Amazonian foreland basin and northern plains of Brahmaputra went through regular avulsions with avulsion frequency interval between a decade to few years (Lombardo 2016, Sah and Das 2018). If we look at our avulsion data, it reveals several HFR rivers with high avulsion frequencies (Table 2). We listed eight rivers with an average avulsion recurrence interval of less than three years. This places these rivers of the HFR among the most avulsion-hit rivers in the world. This study supplements the global understanding of river avulsion frequencies.

This work contributed to the factual knowledge about the river avulsion distribution across HFR, one of the most avulsion-prone regions in the world. The avulsion dataset can be further utilized to explore other studies on river avulsion. Such studies include avulsion style, avulsion duration, avulsion length, hop length, etc.

7 Conclusions

The Himalayas form one of the world's largest and most active foreland regions. The ample river avulsion fingerprints along the foreland region open up new research possibilities. We collected a novel dataset on chronological avulsion events in 110 rivers across HFR. The 286 recorded avulsion events identify pockets of avulsion-active areas in the HFR. The majority of the avulsion-affected rivers are located in the eastern belt of the north Brahmaputra plain. We delved into multiple sources – aerial and satellite images, topographical maps, field photographs, interviews with the locals, and previous literature – and identified that the great 1950 Assam earthquake and deforestation over recent decades have been the principal contributors to the frequent avulsions in the rivers in the eastern belt of Brahmaputra plain.

We find that the smaller rivers of HFR are more susceptible to avulsion events. Nearly 80% of the avulsion-affected rivers (≥ 6 avulsion events) originate in or below the southern part of the lesser Himalayas. Those active rivers have catchment areas of less than 500 km^2, strengthening the observation. Our observations pointed out two major factors contributing to the higher avulsion in smaller rivers. They are the non-incised channel, especially along the avulsion-hit reaches of the smaller rivers, and their rapid morphological transition (from a braided to a meandering channel pattern).

The longitudinal distribution of avulsions along the study rivers identified transitional reaches and proximal areas as the most active sections. This contrast is associated with the depositional environments of the river basins in their upper sandy facies and lower muddy facies. It essentially controls their channel patterns and bed sedimentation and decides the frequency of avulsion events. We also noticed that the rivers with abrupt shifts from braided to meandering channel patterns (in their transition reaches) are more prone to avulsion activities with nodal characteristics in a few cases.

We identified river avulsion-active belts in the HFR. Considering the short recurrence intervals of the rivers, the identified active belts can be important sites for future studies, especially for assessing processes and mechanisms associated with avulsion in foreland regions.

Acknowledgements

The first author is an awardee of the Council of Scientific and Industrial Research (CSIR) research associateship [HRDG (CSIR) vide sanction letter no./file no.: 09/079(2836)/2019-EMR-I]. The author acknowledges CSIR for the same. The authors gratefully acknowledge the United States Geological Survey (USGS) as the source of the Landsat and Sentinel images, Corona satellite photographs, and SRTM DEM data. Topographical maps of the Survey of India are used in this work, for which we acknowledge the Survey of India. The authors acknowledge the CHIRPS research communities for the data. This work also uses high-resolution data (LISS IV images) procured under the DST-SERB sponsored project (SB/EMEQ-108/2013). We acknowledge DST-SERB for the same. The authors thank Dr G. Maitra for checking the manuscript. We acknowledge the Geological Survey of India for the use of tectonic information available at its Bhukosh portal. We are thankful to Rokel Basumatary, Tanuj Tayeng, Dr Jayanta Kumar Baruah, Sanat Kumar Gogoi, and several other persons who provided information about the rivers in the eastern Brahmaputra plain.

Disclosure statement

No potential conflict of interest was reported by the authors.

Funding

This work was supported by the Council of Scientific and Industrial Research [09/079(2836)/2019-EMR-I].

ORCID

D. Nagesh Kumar http://orcid.org/0000-0002-5294-8501

References

Aslan, A., Autin, W.J., and Blum, M.D., 2005. Causes of river avulsion: insights from the late Holocene avulsion history of the Mississippi River, U.S.A. *Journal of Sedimentary Research*, 75 (4), 650–664. doi:10.2110/jsr.2005.053

Assine, M.L., 2005. River avulsions on the Taquari megafan, Pantanal wetland, Brazil. *Geomorphology*, 70 (3–4), 357–371. doi:10.1016/j.geomorph.2005.02.013

Borgohain, S., *et al*., 2016. Flood hazard assessment of the Jiadhal fan, Assam, India. In: international conference on climate change mitigation and technologies for adaptation. Shillong: Synod College.

Borgohain, S., *et al*., 2017. Structural controls on topography and river morphodynamics in upper Assam valley, India. *Geodinamica Acta*, 29 (1), 62–69. doi:10.1080/09853111.2017.1313090

Brooke, S., *et al*., 2022. Where rivers jump course. *Science*, 376 (6596), 987–990. doi:10.1126/science.abm1215

Chakraborty, T., *et al*., 2010. Kosi megafan: historical records, geomorphology and the recent avulsion of the Kosi River. *Quaternary International*, 227 (2), 143–160. doi:10.1016/j.quaint.2009.12.002

Coleman, J.M., 1969. Brahmaputra river: channel processes and sedimentation. *Sedimentary Geology*, 3 (2–3), 129–239. doi:10.1016/0037-0738(69)90010-4

Coles, D.R. and Klingeman, P.C., 2014. Channel avulsion dynamics in meandering rivers. World Environmental and Water Resources Congress, ASCE, 1475-1485.

Dasgupta, S., *et al*., 2000. Seismotectonic atlas of India and its environs. In: P.L. Narula, S.K. Acharyya, and J. Banerjee, eds. *Geological survey of India*. India: Geological Survey of India, 1–86.

Datta, B. and Singh, V.P., 2004. Hydrology. In: V.P. Singh, N. Sharma, and C.S.P. Ojha, eds. *The Brahmaputra basin water resources*. Dordrecht: Kluwer Academic Publishers, 139–195.

Edmonds, D.A., *et al*., 2016. Avulsion flow-path selection on rivers in foreland basins. *Geology*, 44 (9), 695–698. doi:10.1130/G38082.1

Flam, L., 1993. Fluvial geomorphology of the lower Indus basin (Sindh, Pakistan) and the Indus civilization. In: J.F. Shroder Jr, ed. *Himalaya to the sea- Geology, geomorphology and the Quaternary*. London and New York: Routledge, 166–180.

Fuller, I.C., Reid, H.E., and Brierley, G.J., 2013. Methods in geomorphology: investigating river channel form. In: J. Shroder Editor in Chief, A. D. Switzer, and D.M. Kennedy, eds. *Treatise on geomorphology*. San Diego, CA: Academic Press, 73–91.

Goswami, D.C., 1985. Brahmaputra river, Assam, India: physiography, basin denudation and channel aggradation. *Water Resources Research*, 21 (7), 959–978. doi:10.1029/WR021i007p00959

Gupta, N., *et al*., 2014. One-dimensional modeling of a recent Ganga avulsion: assessing the potential effect of tectonic subsidence on a large river. *Geomorphology*, 213, 24–37. doi:10.1016/j.geomorph.2013.12.038

Jain, V. and Sinha, R., 2003. Hyperavulsive-anabranching Baghmati River system, north Bihar plains, eastern India. *Zeitschrift für Geomorphologie*, 47 (1), 101–116. doi:10.1127/zfg/47/2003/101

Jones, L.S. and Schumm, S.A., 1999. Causes of avulsion: an overview. In: N.D. Smith and J. Rogers, eds. *Fluvial sedimentology VI*. Vol. 28. Oxford: Blackwell Science Ltd, 171–178.

Lahiri, S.K. and Sinha, R., 2012. Tectonic controls on the morphodynamics of the Brahmaputra River system in the upper Assam valley, India. *Geomorphology*, 169-170, 74–85. doi:10.1016/j.geomorph.2012.04.012

Lahiri, S.K. and Sinha, R., 2014. Morphotectonic evolution of the Majuli island in the Brahmaputra valley of Assam, India inferred from geomorphic and geophysical analysis. *Geomorphology*, 227, 101–111. doi:10.1016/j.geomorph.2014.04.032

Larkin, Z.T., *et al*., 2017. Timescales, mechanisms, and controls of incisional avulsions in floodplain wetlands: insights from the Tshwane River, semiarid South Africa. *Geomorphology*, 283, 158–172. doi:10.1016/j.geomorph.2017.01.021

Li, J., *et al*., 2022. Upstream migration of avulsion sites on lowland deltas with river-mouth retreat. *Earth and Planetary Science Letters*, 577, 117270. doi:10.1016/j.epsl.2021.117270

Lombardo, U., 2016. Alluvial plain dynamics in the southern Amazonian foreland basin. *Earth System Dynamics*, 7 (2), 453–467. doi:10.5194/esd-7-453-2016

Makaske, B., 2001. Anastomosing rivers: a review of their classification, origin and sedimentary products. *Earth-Science Reviews*, 53 (3–4), 149–196. doi:10.1016/S0012-8252(00)00038-6

Mitra, D., Tangri, A.K., and Singh, I.B., 2005. Channel avulsions of the Sarda River system, Ganga plain. *International Journal of Remote Sensing*, 26 (5), 929–936. doi:10.1080/0143116031000102458

Morozova, G.S. and Smith, N.D., 1999. Holocene avulsion history of the lower Saskatchewan fluvial system, Cumberland Marshes, Saskatchewan-Manitoba, Canada. In: N.D. Smith and J. Rogers, eds. *Fluvial sedimentology VI*. Vol. 28. Oxford: Blackwell Science Ltd, 231–249.

Patel, A., *et al*., 2021. Rainfall variability over the Indus, Ganga, and Brahmaputra River basins: a spatio-temporal characterization. *Quaternary International*, 575-576, 280–294. doi:10.1016/j.quaint.2020.06.010

Poddar, M.C., 1950. The Assam earthquake of 15th August, 1950. *Indian Miner*, 4 (4), 167–176.

Ramakrishnan, D., Bandyopadhyay, A., and Kusuma, K.N., 2009. SCS-CN and GIS-based approach for identifying potential water harvesting sites in the Kali watershed, Mahi River basin, India. *Journal of Earth System Science*, 118 (4), 355–368. doi:10.1007/s12040-009-0034-5

Restrepo, J.D., Kettner, A.J., and Syvitski, J.P.M., 2015. Recent deforestation causes rapid increase in river sediment load in the Colombian Andes. *Anthropocene*, 10, 13–28. doi:10.1016/j.ancene.2015.09.001

Roy, A.B., 2014. Indian subcontinent. In: R.C. Selley, L.R.M. Cocks, and I. R. Plimer, eds. *Encyclopedia of geology*. Oxford: Elsevier, 285–296. doi:10.1016/B0-12-369396-9/00396-8

Sah, R.K. and Das, A.K., 2018. Morphological dynamics of the rivers of Brahmaputra. *Journal of the Geological Society of India*, 92 (4), 441–448. doi:10.1007/s12594-018-1039-y

Sah, R.K., Kumar, D.N., and Das, A.K., 2022. Channel evolution of the Himalayan tributaries in northern Brahmaputra plain in recent centuries. *Acta Geophysica*, 70 (3), 1317–1330. doi:10.1007/s11600-022-00780-0

Sarma, J.N. and Phukan, M.K., 2004. Origin and some geomorphological changes of the river island Majuli of the Brahmaputra in Assam, India. *Geomorphology*, 60, 1–19. doi:10.1016/j.geomorph.2003.07.013

Sinha, R., 2005. Why do Gangetic rivers aggrade or degrade? *Current Science*, 89 (5), 836–840.

Sinha, R., 2009. The great avulsion of Kosi on 18 August 2008. *Current Science*, 97 (3), 429–433.

Sinha, R., *et al*., 2019. Basin-scale hydrology and sediment dynamics of the Kosi River in the Himalayan foreland. *Journal of Hydrology*, 570, 156–166. doi:10.1016/j.jhydrol.2018.12.051

Sinha, R. and Friend, P.F., 1994. River systems and their sediment flux, Indo-Gangetic plains, northern Bihar, India. *Sedimentology*, 41, 825–845. doi:10.1111/j.1365-3091.1994.tb01426.x

Sinha, R., Tandon, S.K., and Gibling, M.R., 2010. Shallow sub-surface stratigraphy of the Ganga basin, Himalayan foreland: present status and future perspectives. *Quaternary International*, 227, 81–86. doi:10.1016/j.quaint.2010.07.015

Slingerland, R. and Smith, N.D., 2004. River avulsions and their deposits. *Annual Review of Earth and Planetary Sciences*, 32, 257–285. doi:10.1146/annurev.earth.32.101802.120201

Stouthamer, E., 2014. Avulsion channel. In: H. Hargitai and Á. Kereszturi, eds. *Encyclopedia of planetary landforms*. New Yor: Springer, 102–109.

Syvitski, J.P.M. and Brakenridge, R., 2013. Causation and avoidance of catastrophic flooding along the Indus River, Pakistan. *GSA Today*, 23 (1), 4–10. doi:10.1130/GSATG165A.1

Tooth, S., *et al*., 2007. Chronology and controls of avulsion along a mixed bedrock-alluvial river. *GSA Bulletin*, 119 (3/4), 452–461. doi:10.1130/B26032.1

Valenza, J.M., *et al*., 2020. Downstream changes in river avulsion style are related to channel morphology. *Nature Communications*, 11, 2116. doi:10.1038/s41467-020-15859-9

Wang, Z. and Liang, Z., 2000. Dynamic characteristics of the Yellow River mouth. *Earth Surface Processes and Landforms*, 25, 765–782. doi:10.1002/1096-9837(200007)25:7<765::AID-ESP98>3.0.CO;2-K